EUROPEAN FUSION DEVELOPMENT AGREEMENT

EFDA–JET–PR(03)19

A. A. Korotkov, P. D. Morgan, J. Schweinzer, J. Vince
and JET EFDA Contributors

Line Ratio Method for Measurement of Magnetic Field Vector using Li-Multiplet ($2\,^2S - 2\,^2P$) Emission

Line Ratio Method for Measurement of Magnetic Field Vector using Li-Multiplet ($2\,^2S - 2\,^2P$) Emission

A. A. Korotkov[1], P. D. Morgan[1], J. Schweinzer[2], J. Vince[1]
and JET EFDA Contributors*

[1]Euratom /UKAEA Fusion Association, Culham Science Centre, Abingdon, Oxon., OX14 3DB, UK.
[2]Euratom/IPP Fusion Association, Max Planck Institute für Plasmaphysik, D-85148 Garching, Germany
** See the appendix of JET EFDA contributors (prepared by J. Paméla and E.R Solano),*
"Overview of JET Results",
Fusion Energy 2002 (Proc. 19th Int. Conf. Lyon, 2002), IAEA, Vienna (2002).

Preprint of Paper to be submitted for publication in
Physical Review A

ABSTRACT

A new method has been developed, for use in magnetic confinement devices, to measure the magnetic field vector $\vec{B}$ in plasmas or gases. It utilises the intensities of the π and σ components of the resonance multiplet emitted by lithium atoms subjected to a strong Zeeman effect. A difference in dependence of these intensities on the inclination angle θ between $\vec{B}$ and the line of sight allows one to determine the direction of $\vec{B}$, provided the intensity ratio of the π and σ components $\xi(\theta)$ is measured. The magnitude of $\vec{B}$ is routinely inferred from the width of the multiplet. The principles of the measurement are elaborated in detail for the case of a fast Li-beam (20-100 keV) used to diagnose a fusion plasma. The deviation of the population of the m- states from the statistical one due to a dominant direction for the relative velocity during the excitation of the atoms by plasma ions has been analysed and corrections to $\xi(\theta)$ are calculated. The geometry employed for the measurement is investigated in order to minimise the uncertainties due to systematic and random errors. A procedure for in-situ calibration is outlined. As proof of the principle the results from poloidal magnetic field measurements in ohmic and H-mode pulses on the Joint European Torus (JET) are analysed. As expected, much higher components of the poloidal magnetic field B_Z and B_R have been found at the plasma edge in H-mode pulses indicating the sensitivity of the measurements to the bootstrap current. Reasonable agreement has been observed between the expected and obtained accuracy. The uncertainty in $\xi(\theta)$ is found to be close to the statistical limit at $\xi(\theta) > 6\%$. The prospects for current density measurement at the plasma edge, which remain a key issue for achieving advanced performance of modern tokamaks, are examined in terms of making use of the developed technique. It is concluded that prospects are good provided the best available Li-beam guns, with equivalent neutral current ~5mA, are used.

1. INTRODUCTION

Measurement of the current profile at the plasma edge in modern tokamaks remains a key issue for investigating the physics of ELMs and achieving advanced performance. Existing methods based on polarisation measurements [1,2] require that the initial direction of polarisation is maintained. This is difficult, as the image is transmitted through a significant thickness of glass and thus subject to Faraday rotation depending on the plasma magnetic field [3].

We have developed an alternative method [4] based on measurement of the intensity ratio of the π and σ components of the Li-multiplet ($2\,^2S - 2\,^2P$) emitted by a neutral Li-beam. The technique utilises a difference in dependence of these intensities on the inclination angle between the total magnetic field vector $\vec{B}$ and the line of sight. The method does not require a polarisation measurement but can provide similar accuracy to the Motional Stark Effect diagnostic (MSE) for the inclination angle, ~0.2^o. An important advantage of the proposed approach is that there is no interference from the plasma radial electric field.

In the paper we elaborate the principles of the measurement (section 2). Basic relationships between measured parameters and components of $\vec{B}$ are deduced in section 2.2. Section 2.3 is devoted

to calculation of the polarisation of the radiation and possible systematic errors. Error propagation and optimal geometry are considered in section 2.4. The calibration procedure is outlined in Appendix 3.

As a proof of the principle we analyse the results of the poloidal (B_p) magnetic field measurements in ohmic and H-mode pulses on the Joint European Torus (JET). The method is applied in full for B_Z measurement. B_R is derived using additional information on the magnitude of the toroidal magnetic field B_T due to simplified geometry used. Section 3.1 outlines the experimental setup. Evaluation procedure for B_Z and B is described in section 3.2. Results of the measurements are presented in section 3.3. Obtained accuracy is compared with predictions in section 3.4. Prospects for current density measurement are discussed in section 4. Section 5 contains conclusions and recommendations on using the developed method.

2. PRINCIPLE OF THE MEASUREMENT

2.1 Li (2 ^{2}S - 2 ^{2}P) MULTIPLET IN TOKAMAK PLASMAS

In plasmas produced in modern tokamaks the 2p jm_j – states of the lithium atom are subject to very strong mixing (Paschen-Back effect) in the magnetic field B, due to $\eta = B/B_0 >> 1$, where $B_0 = A_{FS} / 2\mu_B = 0.24$ Tesla, $A_{FS}=2.8\times10^{-5}$ eV is the fine splitting parameter for the 2p ^{2}P- states and μ_B is the Bohr magneton. As a result the relatively simple Zeeman pattern of the allowed 2 ^{2}S – 2 ^{2}P- transitions forms a Lorentz triplet (Fig.1). The central peak is due to π- transitions, while the two flank peaks are nearly pure σ- transitions. The relative intensities in the multiplet are accurately simulated for arbitrary values of the parameter η [5]. The last is due to the central type of potential for the optical electron in lithium and high accuracy of all the parameters involved. The uncertainty in the A_{FS} (~5%) is not so important in the case of the Paschen-Back effect.

An important advantage of using the Li (2 ^{2}S - 2^{2}P) multiplet for the diagnostic is a very weak interference from the electric field. One can estimate the splitting of the 2s ^{2}S and 2p ^{2}P states induced by the electric field $\in$ using a second order correction from perturbation theory:

$$\Delta E_{\gamma jm} = \Delta E_{\gamma' j'm} = \frac{|<\gamma,j,m\,|D_Z\,|\,\gamma',j',m>|^2}{\Delta E_0} \in^2$$
$$= \frac{3e^2\hbar^2}{2m(\Delta E_0)^2} \frac{(2j+1)^2}{2(2\ell+1)} f(\gamma'\rightarrow\gamma) \begin{pmatrix} j\ 1\ j' \\ -m\ 0\ m \end{pmatrix} \in^2 \qquad (1)$$

where ΔE_0 is the splitting for a free atom, $f(\gamma'\rightarrow\gamma)$ is an oscillator strength for the 2p→2s transition, (j 1 j'/ -m 0 m) is a 3j-symbol, γ stands for 1s^2 2s and γ' for 1s^2 2p, $\ell = 1$. Taking 3j-symbols from [5] one has $\Delta E(eV) = 2.7\times10^{-20}$ ($\in$ (V/m))^2 for the biggest splitting between 2s^{2}S$_{1/2\ 1/2}$ and 2p ^{2}P$_{3/2\ 1/2}$ states. The strongest electric field $\in_L$ is induced by motion of the beam atoms through the magnetic field of the tokamak (Lorentz electric field). The background radial electric field is a few percent of $\in_L$. For the typical parameters E_{beam}= 10 keV/amu, B = 3 Tesla one has $\in_L = 4.4\times10^5$ B $\sqrt{E_{beam}} = 4.2\times10^6$ V/m. The last gives $\Delta E(eV) = 4.7\times10^{-7} << A_{FS}$. Corresponding corrections to the relative intensities inside the multiplet $\sim (\Delta E/A_{FS})^2 \approx 3\times10^{-4}$.

2.2 INTENSITY RATIO OF THE π AND σ COMPONENTS AND DIRECTION OF THE MAGNETIC FIELD VECTOR

The intensities of the π and σ components have essentially different angle distribution: $J_\pi(\theta) \sim \sin^2\theta$, $J_\sigma(\theta) \sim 1+\cos^2\theta$, where θ is the inclination angle of the line of sight to the total magnetic field vector $\vec{B}$. Measurement of $\xi(\theta) = J_\pi(\theta) / J_\sigma(\theta)$ for a localised light source (beam atoms) provides a determination of the direction of $\vec{B}$.

In the general case two components of B_P (B_Z, B_R) and B_T must be determined simultaneously. This implies measurement of ξ(θ) at two inclination angles. An example of sight lines and beam trajectory is presented in Fig.2. The Li-beam is injected from the top port along a vertical line. Radiation from the Li-beam is detected from points z_i along the beam direction using two periscopes with turning mirrors M_1 and M_2. The beam is in the optical planes of the periscopes.

Components of the magnetic field are determined from scalar products of $\vec{B}$ and line-of-sight unit vectors $\vec{\ell}_i$ in which $\cos\theta_i$ is input from the measurements and the magnitude of B is measured from the splitting of the σ- peaks[1]:

$$B\cos\theta_i = B_T \ell_{T_i} + B_R \ell_{R_i} + B_Z \ell_{Z_i} \qquad (2)$$

$$\xi(\theta_i) = \frac{Ck\sin^2\theta_i}{1+k\cos^2\theta_i} \quad , \qquad i = 1,2 \quad , \qquad (3)$$

$$B^2 = B_T^2 + B_R^2 + B_Z^2 \qquad , \qquad (4)$$

$$\ell_T = \cos\beta\cos\varphi,\ \ell_R = \cos\beta\sin\varphi,\ \ell_Z = -\sin\beta$$

In Appendix 1 we show that despite the quadratic nature of Eq.(4) no uncertainty arises if the geometry of observation is chosen properly.

All parameters in Eqs. (2)-(3) are known. Geometry parameters β, φ and *k*, the ratio of mirror reflectivity for P and S polarisation, are derived following calibration in gas (Appendix 3). The polarisation correction C is described below.

Notice the special cases $|B_R \ell_R / B_Z \ell_Z| \ll 1$ or $\gg 1$, when only one periscope is required to measure B_Z or B_R respectively. The first is the most interesting case which is relevant to measurement in the magnetic midplane ($|B_R / B_Z|$) << 1). It also corresponds to the geometry used on JET ($|\ell_R / \ell_Z| \ll 1$).

2.3 POLARISATION OF THE Li (2s ^{2}S - 2p ^{2}P)- RADIATION

Special consideration is required for the polarisation correction $C = (1+\Pi) / (1-\Pi)$, where Π is the polarisation. We notice that the polarisation is a general feature of the radiation of the beam atoms due to the existence of a dominant direction for the relative velocity during the excitation of the atoms by plasma ions ($\vec{v}_{rel} = \vec{v}_{beam} - \vec{v}_i \approx \vec{v}_{beam}$, since $v_{beam} \gg v_i$, where $\vec{v}_i$ is thermal velocity of the plasma ions). Under such circumstances the population of the m-states keeps the features of the

[1] Eq.(3) is valid for small angles φ with accuracy $\max\{\sin^2\varphi,\ 2\,(B_R/B_T)\tan\varphi,\ (B_R/B_T)^2\}$ or at any φ if k = 1. The relationship between the measured parameter ξ(θ) and cosθ in the general case is presented in Appendix 2.

excitation process, namely: at low velocity $v << v_0 = \sqrt{2I}$ the electron manages to follow the disturbing Coulomb field during the collision (v_0 is orbital velocity of the electron in the final state with ionisation potential I in atomic units). Since the disturbing field is directed along the same axis before and after the collision the electron maintains the initial orientation of its orbit, that is the $\Delta m=0$- transition predominantly occurs. In our case it means a predominant population of the 2p m=0 state in the beam frame. This is the reason for the polarisation of the 2s ^{2}S - 2p ^{2}P- radiation. At $v >> v_0$ the collision axis rotates too fast for the electron to follow, resulting in equal population of all possible m-states (statistical population). As a result Π goes to zero.

We have calculated the relative population P^i_m of the 2pm- states due to excitation of the lithium by protons as a function of the relative velocity. Using the results presented in Appendix 4 we calculate the effective excitation rate to the 2pm- state due to collisions with electrons and ions as:

$$<\sigma v>_m = \frac{<\sigma v>_e}{2\ell + 1}\left(1 + (2\ell + 1)\frac{<\sigma v>_i}{<\sigma v>_e} P^i_m\right) \tag{5}$$

where $<\sigma v>_e$ and $<\sigma v>_i$ stand for rate coefficients for 2s-2p excitation by electrons and ions presented in review [6], $\ell = 1$[2]. For the relative population of the 2pm-states one has:

$$P_m = \frac{<\sigma v>_m}{\sum_m <\sigma v>_m} = \frac{1}{3}\,\frac{1+3\,\frac{<\sigma v>_i}{<\sigma v>_e} P^i_m}{1+\frac{<\sigma v>_i}{<\sigma v>_e}} \tag{6}$$

In Eqs. (5) and (6) we take into account that electrons produce an equal population for all m- states and $\sum_m P^i_m = 1$. With P_m known the calculation of the polarisation is straightforward:

$$\Pi = \frac{\sum_m (|<m|D_0|0>|^2 - |<m|D_1|0>|^2) P_m}{\sum_m (|<m|D_0|0>|^2 + |<m|D_1|0>|^2) P_m}\,, \tag{7}$$

where $<m|D_q|0>$ is the angle part of the dipole momentum for transition with $\Delta m = q$, $m = 0,\pm 1$. The result is:

$$\Pi_{\|} = 3\,\frac{2P_0 - P_1}{14P_0 + 11P_1}\,, \qquad \Pi_{\perp} = -3\,\frac{2P_0 - P_1}{25P_0 + 22P_1} \tag{8}$$

where $P_1 = P_{-1} + P_{+1}$. $\Pi_{\|}$ and $\Pi_{\perp}$ is the polarisation for the beam injected along and perpendicular to $\vec{B}$. In the last case Π decreases due to projection of the m=0 states from the beam frame into |m|=1- states in the frame with quantisation axis directed along $\vec{B}$. The results are presented in Fig.3. The polarisation is found to be small at $E_{beam} > 50$ keV. Perpendicular injection of the beam is beneficial for reduction of the polarisation. Π is smaller in cold plasma due to the "depolarisation" effect of the electron excitation.

The polarisation if not measured results in systematic error $\Delta\theta_\Pi$ for the inclination angle. From Eq.(3) we have:

[2] Notice that collisional mixing of the 2pm- states is not effective due to small rate coefficients for $\Delta\ell$=0- transitions in the far Born range.

$$\Delta\theta_{\Pi} = \frac{\tan\theta\ (1+k\cos^2\theta)}{(1-\Pi^2)\,(k+1)}\,\Delta\Pi \tag{9}$$

The error $\Delta\theta_{\Pi}$ is presented in Fig.4. The uncertainty of the polarisation $\Delta\Pi$ is taken into account according to the variation of Π in the electron temperature interval 100 - 1000 eV (Fig.3). One can see that the systematic error due to unknown polarisation is small ~ 0.1^o if $\theta \le 40^o$.

2.4 OPTIMAL GEOMETRY

The accuracy of the measurement depends on the sensitivity of the ratio ξ to B_p and the accuracy of the measurement of ξ itself. Both factors depend on the geometry used and direction of $\vec{B}$. To investigate this dependence we solve equations (2), (3) for the limiting cases $|B_R \ell_R / B_Z \ell_Z| << 1$ or $>> 1$. The result is:

$$B_s = B_T\ \frac{\ell_T\ \ell_s - \chi_s F\sqrt{\ell^2_T + \ell^2_s - F^2}}{F^2 - \ell^2_s}\ , \tag{10}$$

where F = cosθ, s = Z or R for B_Z - or B_R - measurement respectively. For the geometry of Fig.2 , $\chi_Z = -1$, $\chi_R = +1$, $\ell_T > 0$.

Taking into account that $F = \sqrt{\frac{1-\xi}{1+\xi}} = \frac{\ell_T + \eta_s \ell_s}{\sqrt{1+\eta_s^2}}$, where $\eta_s = \frac{B_s}{B_T}$, one has[3]

$$\frac{\Delta B_s}{B_s} = \frac{\partial \ell n B_s}{\partial \ell n \xi}\ \frac{\Delta\xi}{\xi} = \Phi\,(\eta_s, \beta, \varphi)\ \frac{\sqrt{\xi}}{1+\xi}\ \frac{\Delta\xi}{\xi} \tag{11}$$

where $\Phi\,(\eta_s, \beta, \varphi) = \frac{\sqrt{1-F^4}}{2\eta_s F\,(F^2 - \ell_s^2)}\left(\frac{\ell_T^2 + \ell_s^2 - 2F^2}{\sqrt{\ell_T^2 + \ell_s^2 - F^2}} + 2\,\chi_s\,\eta_s\,F\right)$

For further investigation we assume that uncertainty $\Delta\xi$ is determined by Poisson statistics of the counts collected. In this case $\frac{\Delta\xi}{\xi} = \frac{1+\xi}{\sqrt{\xi}}\ \frac{1}{\sqrt{N_\Sigma}}$, where N_Σ is the total number of counts collected for $\pi-$ and $\sigma-$ components during the measurement Notice that N_Σ does not depend on the geometry since the total intensity of the multiplet has an isotropic angle distribution at C = 1.

Then $\frac{\Delta B_s}{B_s} = \Phi\,(\eta_s, \beta, \varphi)\ \frac{1}{\sqrt{N_\Sigma}}$.

$\Phi(\eta_s, \beta, \varphi)$ must be minimised to obtain the smallest error in the measurement of the B_s. The $\ell n\{|\Phi(\eta_s, \beta, \varphi)|\}$ is presented in Figs.5-8. As expected results for B_Z and B_R are effectively symmetric in respect to the replacement of β with φ.

An explanation is required for the observed increase of the absolute value of $\Phi(\eta_s, \beta, \varphi)$ at some angles at $\ell_S\eta_S/\ell_T > 0$ (Fig.7 and Fig.8). These cases correspond to $\ell_T^2 + \ell_S^2 - F^2 = (\ell_S - \eta_S\ell_T)^2 \to 0$ in the formula for $\Phi(\eta_s, \beta, \varphi)$. Since $\sqrt{\ell_T^2 + \ell_S^2}$ is a cosine of the angle between $\vec{\ell}$ and the $(\vec{B}_T, \vec{B}_s)$ -

[3] For the general case we omit the details of the optics assuming k = 1 and take also into account that C≈1.

plane one concludes that this is the observation when the projection of $\vec{\ell}$ onto this plane is parallel to $\vec{B}$. Bad conditions occur at $\tan\beta = -\eta_Z \cos\varphi$ and $\tan\varphi = \eta_R$ in Fig.7 and Fig.8 correspondingly. The conditions include the observation along or perpendicular to $\vec{B}$ as limiting cases.

The loss of the sensitivity of the ξ to B_s can be explained from the Eq.(2) directly. We rewrite (2) as $F = \sqrt{\ell_T^2 + \ell_S^2}\cos(\alpha-\delta)$ where $\tan^{-1}(\alpha) = \ell_S / \ell_T$ and $\tan^{-1}(\delta) = \eta_s$. Since $\partial F/\partial\delta \sim \sin(\alpha-\delta)$, the cosine of the inclination angle loses the sensitivity to changes of B_s at $\alpha = \delta$.

We conclude that for B_Z- measurement the lines of sight should have parameters: $\varphi \le 10^0$, $\eta_Z < \beta \le 40^0$ ($\beta \le 10^0$, $\eta_R < \varphi \le 40^0$ for B_R- measurement)[4]. The condition $\beta \le 40^0$ is also beneficial for reduction of the systematic error due to polarisation of the radiation (Fig.4). The cases of parallel projection of the line of sight onto the plane where $\vec{B}$ changes should be avoided. It is enough to provide

$$\eta_S \ell_S / \ell_T < 0 \tag{12}$$

Notice that condition (12) provides also the beneficial increase in ξ with increasing B_s. In the opposite case an additional error can arise if a deconvolution procedure has to be applied for inferring the π to $\sigma-$ ratio at small ξ (see section 3.2).

In the end we present the modified formula (11) for $\Delta B_Z/B_Z$ taking into account reflectivity of the mirror $k \neq 1$. At small φ one has:

$$\frac{\Delta B_Z}{B_Z} = f(k)\ \Phi(\eta_Z, \beta, \varphi)\ \frac{\sqrt{\xi}}{1+\xi}\ \frac{\Delta\xi}{\xi} \tag{13}$$

where $f(k) = \sqrt{(k+1)/[k(\xi+2) - \xi]}$. Reduction of the reflectivity for the $\pi-$ component ($k < 1$) results in an increase of the error by a factor $\sqrt{(k+1)/2k}$ at $\xi \ll 1$. For the present measurement on JET ($k \sim 0.6$) the error increases by ~15%.

3. REALISATION OF THE MEASUREMENT ON JET

3.1 EXPERIMENTAL SETUP

The line-ratio method has been applied to the measurement of B_Z and B_R in a number of JET shots using the Li-beam system intended for electron density measurement. The JET Li-beam gun, a version of the ASDEX gun [8], provided 0.05-0.2mA of equivalent neutral current at atom energy E_{beam} = 20-30keV. The Li-beam was injected from the top port in octant 7 along a vertical line (R=3.25m). Only one periscope was used to observe the plasma in the toroidal direction ($\varphi = 1.57^0$) as shown in Fig.2 (periscope 1). Nine fibres of the periscope were connected to a high resolution grating spectrometer SPEX1.25m (F = 9) equipped with a CCD camera. Four fibres were looking at the beam line and five more fibres had sight lines shifted by 2cm from the beam line in the major radius direction. The spectrometer provided wavelength resolution of 0.33Å at étendue é = 1×10^{-5} cm^2 sr. The measurements were carried out over a distance of 16cm along the beam line with spatial resolution of ±1 cm. The investigated area included the scrape-off layer (SOL) and a region inside the separatrix.

[4] β and φ are in radians when compared with dimensionless parameters η_Z or η_R.

The π to σ– ratio ξ was sensitive to B_Z only due to $|\ell_R/\ell_Z| < 0.1$ and $|B_Z| \approx |B_R|$ along the beam line. Therefore we deduced B_Z. Then $|B_R|$ was calculated from $|B_R| = \sqrt{B^2 - B_T^2 - B_Z^2}$. B_T and the sign of B_R were taken from the JET version of the EFIT (Equilibrium Fitting) code [9].

$\ell n\{|\Phi(\eta_z, \beta,)|\}$ for the periscope is shown in Fig.9. It is the case with possible loss of sensitivity presented in Fig.7: $\ell_z \eta_z / \ell_T > 0$. Nevertheless the geometry is close to optimal for B_Z- measurements. The range of poor sensitivity is mostly below the interval of the angles β in use. The sensitivity becomes worse for the outmost channels (the lowest β) at high $|\eta_z| \geq 0.2$ only.

3.2 EVALUATION OF B_z AND B FROM THE MEASURED Li-MULTIPLET

Typical spectra recorded with exposure time 1sec are shown in Fig.10. The Li-multiplet is reliably observed in four channels looking at the beam. Traces of the emission are also observed in the shifted channels due to the width of the beam in the radial direction, about 3cm.

Doppler shifts of the emission due to different observation angles β for different channels are clearly seen. Another consequence of the Doppler effect is an additional broadening of the peaks. It happens because of the finite aperture of the optics $\Delta\beta$: $\Delta\lambda_D = (v_{beam}\lambda/c)\cos\beta\,\Delta\beta$. The channels have an aperture of 1.0^0-1.3^0 that gives 0.32-0.44Å of additional width to the peaks at half maximum. The broadening complicates the identification of the π-peak. The following deconvolution procedure has been applied to evaluate B_Z and B.

The measured multiplet is described by a 6-parameter-fitting function:

$$J(\lambda) = A_3 + A_0 \left(\xi(A_5) \sum_{i=1}^{4} I_\pi^i(\Delta\lambda_\pi^i(A_4), A_4) + \sum_{i=1}^{6} I_\sigma^i(\Delta\lambda_\sigma^i(A_4), A_4) \right), \qquad (14)$$

where $I_{\pi,\sigma}(\Delta\lambda) = I_{0\pi,\sigma} \exp(-(\Delta\lambda_{\pi,\sigma})^2/2A_2^2)$, $\Delta\lambda = \lambda - \lambda_0$, $\lambda_0 = A_1 + \Delta\lambda_c(A_4)$,
A_0 is the total intensity of σ-components, A_1 is the wavelength of the multiplet centre, A_2 is a peak width parameter, A_3 is intensity of background, A_4 represents B and A_5 represents B_Z, $\xi(A_5)$ is π to σ– ratio-function (2.3) from Appendix 2.

The function (14) is a sum of all 10 components of the Li multiplet ($2\,^2S$ - $2\,^2P$) plus constant background. The relative intensities of the components $I_{0\pi,\sigma}$ and their wavelength positions $\Delta\lambda_c$ are found from the solution of the eigenvalue problem for 2s and 2p- states [5].

All parameters, including B, are varied step by step over a range of values to minimise, $M = \sum_{r=1}^{n} (J_{exp}(\lambda_r) - J(\lambda_r))^2$ where $J_{exp}(\lambda_r)$ is a measured spectrum (Least squares method). Standard deviations of the parameters are estimated from the error matrix $\Delta(A_i) = (s^2\, C_{ii}^{-1})^{1/2}$, $C_{ij} = \frac{\partial^2 M_{min}}{2\partial A_i\, \partial A_j}$. Dispersion of the measurement s^2 is estimated as $s^2 = M_{min}/(n-p)$, where p = 6 is the number of parameters of the fitting function, n is the number of pixels under the multiplet.

Inside the procedure we used angles β measured from the Doppler shifts. The parameter $k = k_{//}/k_\perp$ for the nickel mirror of the periscope was measured at incidence angle of 45^o. For other incidence

angles we used the k calculated from classical electromagnetic theory of reflection [10] normalised to the measurement at 45^o. The measured $k_{//}$ and $k_{\perp}$ were smaller than the calculated ones by 4% and 30% respectively.

The polarisation correction has been calculated as described in Chapter 2.3: C = 0.92 for E_{beam} = 20keV and C = 0.94 for E_{beam} = 30keV. An example of the deconvolution results is presented in Fig.11.

3.3 RESULTS OF THE MEASUREMENT

As a proof of the developed principles we have applied the π to $\sigma-$ ratio method to the measurement of the magnetic field on JET. Despite not optimised Li-beam performance we intended to get important information on uncertainties that would allow us to analyse the perspective. Moreover, to test the sensitivity to the bootstrap current at the plasma edge was of great importance. The measurements were carried out in the vicinity of the separatrix in ohmic and ELMy H-mode pulses. An essential difference in the poloidal magnetic field at the plasma edge was expected due to the bootstrap current induced by the much bigger pressure gradient in the H-mode shots. Pulses with very infrequent ELMs have been chosen. Nevertheless in most of the shots the results are averaged over a few ELM periods due to our restricted time resolution ~1sec. Some results are presented in Figs. 12-15.

Smooth time behaviour of B_P and its components is usually observed for all spatial points in ohmic pulses. Small variation in the ~10cm area inside the separatrix is also found. On the contrary, in H-mode shots the time behaviour of B_P for points at the separatrix and 7cm inside looks different even after averaging over a few ELM events. The magnitude of B_P is often higher at the separatrix than inside. The results imply redistribution of a significant part of the current near the separatrix in H-mode pulses.

More detailed information is revealed when the time interval between ELMs approaches the exposure time. Figure 15 demonstrates the big difference between B_P measured at two points inside the separatrix just before the type I ELMs. This difference is clearly seen before the first ELM. It is masked during the ELMy period due to averaging over ELMs. The feature is regained in a long ELM-free period 19.5-21.5s. Significant current density at the plasma edge before the type I ELM would be a natural suggestion from the observation.

We have compared our results with the equilibrium fitting code EFIT based on magnetic measurements with external coils & loops. Rough agreement is observed for B_R ($B_R = -\sqrt{B^2-B_T^2-B_Z^2}$) in ohmic pulses (Fig.14a). B_Z systematically exceeds the value derived by EFIT (Fig.14a,b). In H-mode pulses both components exceed the EFIT values (Fig.14b). Also, EFIT does not reveal the big spatial variations of the poloidal magnetic field near the separatrix observed before the type I ELMs (Fig.15).

3.4 ANALYSIS OF ACCURACY

We have estimated the standard deviation of ξ from our measurement: $\Delta\xi = (\xi(B_Z-\Delta B_Z)-\xi(B_Z+\Delta B_Z))/2$, where $\xi(B_Z\pm\Delta B_Z)$ is the π to $\sigma-$ ratio function (2.3) from Appendix 2, ΔB_Z is the standard deviation

for B_Z from the deconvolution procedure. The result is compared with predictions based on the statistical origin of the errors in Fig.16. The uncertainties approach the statistical limit at $\xi > 0.06$. At smaller ξ the contribution of the deconvolution procedure dominates due to difficulties in identifying the π- peak. To clarify this contribution we have also estimated $\Delta\xi$ for the case of good identification of the π- peak. The last is the measurement of the multiplet for cold lithium atoms not having any noticeable Doppler broadening of the peaks. During beam commissioning, small flakes of lithium occasionally became detached from the injector and entered the plasma. These resulted in localised intense emission from the cold atoms presented in Fig.17[5]. In the case of good separation of the π and $\sigma-$ peaks $\Delta\xi$ is much smaller for all measured ξ. At $\xi \geq 0.06$ the statistical limit is reached unlike the case of beam atoms where it is still about 2 times higher. Notice that the measurement with good separation of the peaks (as in Fig.17) can be provided for the beam atoms if the aperture of the optics is reduced by a factor of 2.

We have also tested the predictions for the influence of the geometry on the accuracy of the measurement made in section 2.4. The comparison of the calculated $\ell n(|\Phi|)$ with estimation from the measurement is presented in Fig.18. We found a reasonable description of the experimental results by the theoretical approach developed. Notice that this conclusion does not depend on the origin of the uncertainty $\Delta\xi$.

Figure 19 presents the accuracy for B_Z and the inclination angle θ achieved in our measurements. The best values $\Delta B_Z = 0.025$T and $\Delta\theta = 0.5^0$ have been obtained from the multiplet of cold lithium at $N_\Sigma = 5300$. Comparison with the results from the measurements with Li-beam atoms allows one to derive the following relation between ΔB_Z and parameters of the measurement:

$$\Delta B_Z\,(T) = \frac{8\times 10^{-6}\, B_T\,(T)\,\Phi\eta_Z}{\sqrt{i^0_{Li}\,(mA)\;\acute{e}(cm^2\;sr)\;\gamma\,\Delta t(s)}}\,, \qquad (15)$$

where i^0_{Li} is the equivalent neutral current of the injector, γ is the sensitivity of the detection for light with wavelength 6708Å, Δt is the exposure time, Φ is the geometric function presented in section 2.4 (notice that $(\Phi\,\eta_Z)$ is a very weak function of η_Z) .

The reduction of the aperture by a factor of 2 is implicit in Eq. (15) to eliminate the uncertainty induced into the measurement of ξ by the deconvolution procedure. Eq.(15) is valid at $\xi \geq 0.06$ when the statistical limit of the uncertainties is shown to be reached (Fig.16). Notice that Eq.(15) implies measurement with a spatial resolution $\pm$1cm.

4. PROSPECTS FOR CURRENT DENSITY MEASUREMENT

Current density is determined from the measurement of the spatial distribution of the poloidal magnetic field components B_s using Ampere's law: $j_T = -\partial B_Z/\partial R + \partial B_R/\partial Z$. From this relation it is straightforward to estimate the uncertainty in j_T due to the standard deviation of the measured B_s:

$$\Delta j_T\,(A/cm^2) = \frac{10^5}{4\pi}\left(2\,\frac{\Delta B_s\,(T)}{\Delta x\,(cm)}\right), \qquad (16)$$

[5] No deviation of the peak widths from the apparatus function was found. Therefore we concluded that the radiating atoms had the energies below the thermal energy of the plasma ions and called them "cold". Notice that $\Pi = 0$ for the emission of the cold atoms since $\vec{v}_{rel} = \vec{v}_i$ or $\vec{v}_e$ during the excitation process, where v_i, v_e are the thermal velocities of the plasma ions and electrons.

where Δx is a characteristic length for the variation of B_s induced by the bootstrap current at the plasma edge. The last is of order of the Edge Transport Barrier width along the line of sight (Δx ~10cm in JET plasmas at present geometry of the Li-beam system).

We estimate ΔB_s from Eq.(15) keeping all parameters as they were in our measurements except i^0_{Li}= 5mA, étendue = 1×10^{-4} cm^2 sr, Δx = 3cm. The equivalent neutral beam current 3-5mA is provided by ASDEX [8] and DIII-D [11] guns. The étendue of 10^{-4} cm^2 sr can be easily provided by an apparatus with F = 2 (e.g. Fabry-Perot interferometer). Notice that fibre system on JET has much bigger étendue ~1.5×10^{-3} cm^2 sr. From Eq.(16) one has:

$$\Delta j_T\,(A/cm^2) = \frac{4}{\sqrt{\Delta t\,(s)}} \qquad (17)$$

Simulation of the current density distribution at the plasma edge in H-mode pulses [12, 13] implies that Δj ~ 10–20 A/cm^2 would be sufficient to follow the evolution of the current experimentally. We conclude that this accuracy can be provided by the π to $\sigma-$ ratio method at the acceptable exposure time of 40–160 ms. It corresponds to accuracy of 1–2% for the intensity ratio of the π and σ componenets of the Li- multiplet.

CONCLUSION

The new line ratio method for the measurement of the magnetic field vector has been developed and tested. An accuracy of 10– 20% for the poloidal magnetic field components B_Z and B_R and 1% for B has been reached at low effective neutral current of the Li-beam injector 0.05-0.2 mA and low étendue optics (10^{-5} cm^2 sr). Analysis of the Li-flakes emission demonstrates that much better accuracy can be reached provided better separation of the π and $\sigma-$ components in the multiplet is achieved. The last is subject to the optics aperture only.

The method is found to be sensitive to the bootstrap current at the plasma edge in H-mode pulses. We conclude that an accuracy of 10 – 20 A/cm^2, sufficient to follow the evolution of the current experimentally, can be achieved at exposure times of 40 – 160 ms provided the best available Li-beam guns with i^0_{Li} ~ 5mA are used.

When applying the method attention must be given to the geometry employed for the measurement. The cases where the projection of the line of sight onto the plane where $\vec{B}$ changes is parallel to $\vec{B}$ should be avoided. It is preferable to meet the condition (12) and not to use mirrors since they complicate the analysis and decrease the final accuracy.

We emphasise the advantage of high B_T for the better accuracy of the measurement. In our experiments we investigated the interval B_T = 2.2-2.5T. One can expect that an increase of B_T results in an "improvement" of the resolution in the same way as Li-flake emission (Fig.16). It implies that $\Delta\xi/\xi \sim (B_T)^{-1}$.

Two final points:

1) The application of the proposed method with much better time resolution (a few ms) awaits the development of large-diameter alumino-silicate surface ionisation sources [14] which

would provide an order of magnitude higher current density than conventional β-eucryptite sources.

2) An attractive possibility is making use of the emission from a pellet or even intrinsic impurity for the measurement. Our observation of the Li-flake emission models the former. In all cases the angles employed for the measurement must be known with accuracy better than required accuracy for the inclination angle ~0.2^0. In the case of the Li-beam Doppler shifts of the emission provide reliably the required accuracy. In other cases an analysis of the errors due to geometrical uncertainties must be made.

ACKNOWLEDGEMENTS

One of the authors (A. Korotkov) would like to thank Dr. F. Orsito who attracted the attention of the author to the problem of current measurement at the plasma edge in modern tokamaks and Dr. N.C. Hawkes for useful discussions. It is a pleasure to acknowledge a number of clarifying remarks made by Drs W. Morris, A. Murari, G. Matthews and T. Hender.

This work was performed under the European Fusion Development Agreement and was funded jointly by the United Kingdom Engineering and Physical Sciences Research Council and by EURATOM.

REFERENCES

[1]. K. McCormick, Measurement of poloidal field distribution in a tokamak plasma via neutral lithium beam spectroscopy*, Proceedings of the course and workshop*, vol II, 635-656 (Varenna, Italy, 1986).

[2]. F..M. Levinton, *Rev.Sci.Instrum.* **63** (10), 5157-5160 (1992).

[3]. B. C. Stratton, D. Long, R. Palladino and N. C. Hawkes, *Rev. Sci. Instrum.* **70**(1), 898-901 (1999).

[4]. A.A. Korotkov, K. McCormick, P.D. Morgan, J. Schweinzer and J. Vince, Line ratio method for poloidal magnetic field measurement using Li-multiplet ($2\,^2S$-$2\,^2P$) emission, in "Advanced Diagnostics for Magnetic and Inertial Fusion", Proceedings of the International Conference (Varenna, Italy, 2001), 209-212.

[5]. I.I. Sobelmann, *Atomic Spectra and Radiative Transitions* (Springer Verlag, Berlin,1979).

[6]. J.Schweinzer, R. Brandenburg, I. Bray, R. Hoekstra, F. Aumayr, R.K. Janev and H.P. Winter, Atomic Data and Nuclear Data Tables **72**, 239-273 (1999).

[7]. L.D. Landau and E.M. Lifshitz, Quantum Mechanics. Non-relativistic theory, (Pergamon Press, 1977), pp. 213-219.

[8]. K. McCormick, S. Fiedler, G. Kocsis, J. Schweinzer and S. Zoletnik, Fusion Engineering and Design **34-35**, 125-134 (1997).

[9]. D.P. O'Brien, L.L. Lao, E.R. Solano, M. Garriba, T.S. Taylor, J.G. Cordey and J.J. Ellis, Nucl. Fusion **32**, 1351-1360 (1992).

[10]. D. Clarke and J.F. Grainger, Polarized Light and Optical Measurement, (Pergamon Press, 1971), pp. 64-69.

[11]. D.M. Thomas, Rev. Sci. Instrum. **66** (1), 806-811 (1995).

[12]. J.R. Ferron, L.R. Baylor, M.S. Chance et al., Proc. of 27th EPS on Controlled Fusion and Plasma Physics, (Budapest, 2000), Vol. 24B, p.548.

[13]. V. Parail, G. Bateman, M. Becoulet, et. al., 19th IAEA Fusion Energy Conf. (Lyon, 2002) TH/P3-08.

[14]. J.W. Kwan, F.M. Bieniosek, E. Henestroza, et. al., Laser and Particle Beams, **20**, 441-445 (2002).

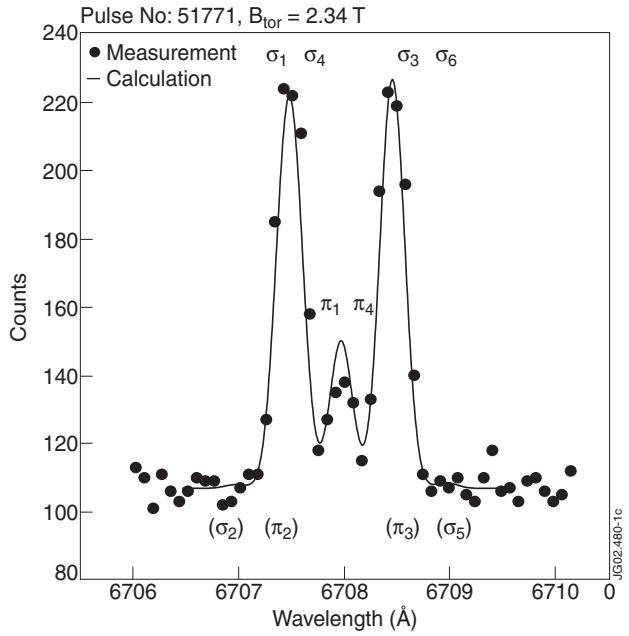

Figure 1: Lorentz triplet of thermal lithium measured on JET.

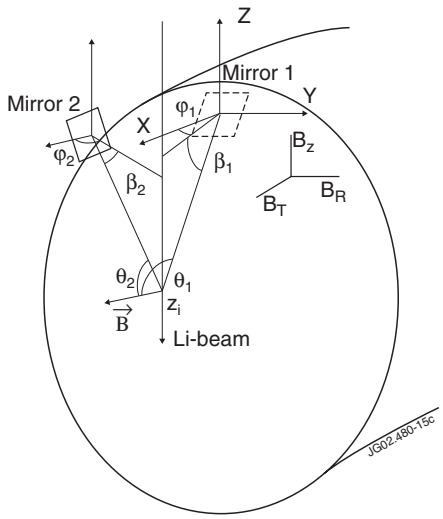

Figure 2: Geometry diagram of the measurement. Toroidal direction is along the X-axis.

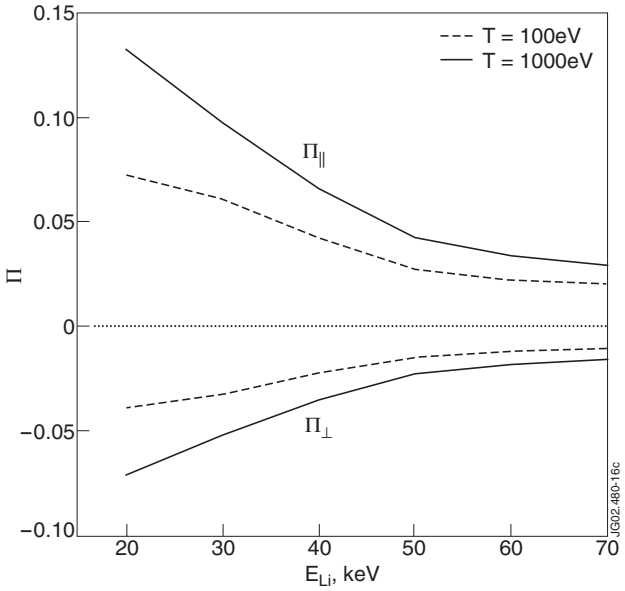

Figure 3: Polarisation of Li(2s ^{2}S 2p ^{2}P) radiation as a function of beam energy and plasma temperature $T=T_e=T_i$.

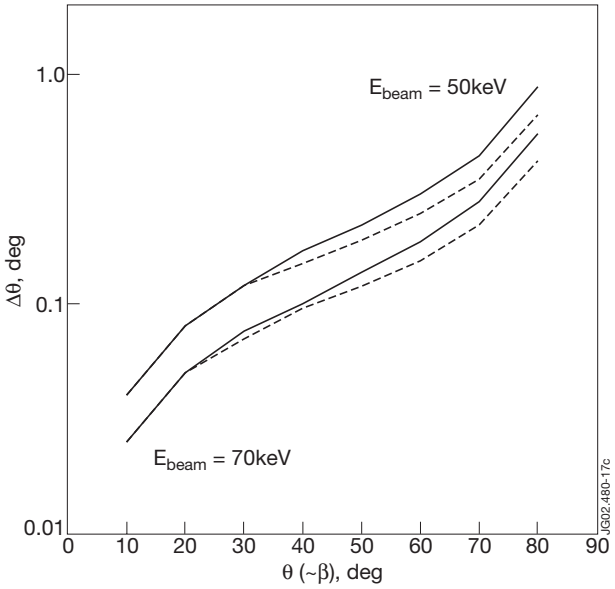

Figure 4: Systematic uncertainty of the measured inclination angle due to variation of $\Pi_\perp$ in the range of T=100-1000 eV. Solid line- k=0.5, dashed line -k =1.

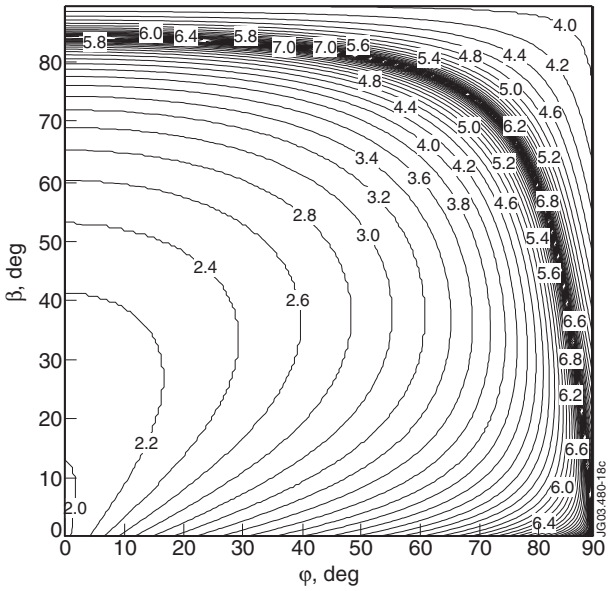

Figure 5: $\mathcal{L}n\ \{|\Phi(\eta_Z, \beta, \varphi)|\}$ at $\eta_Z = 0.1$, $\mathcal{L}_Z\,\eta_Z/\mathcal{L}_T < 0$.

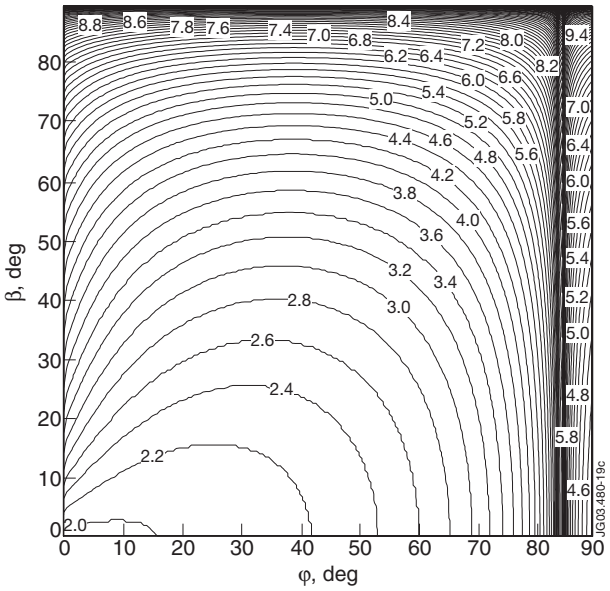

Figure 6: $\mathcal{L}n\ \{|\Phi(\eta_R, \beta, \varphi)|\}$ at $\eta_R = -0.1$, $\mathcal{L}_R\,\eta_R/\mathcal{L}_T < 0$.

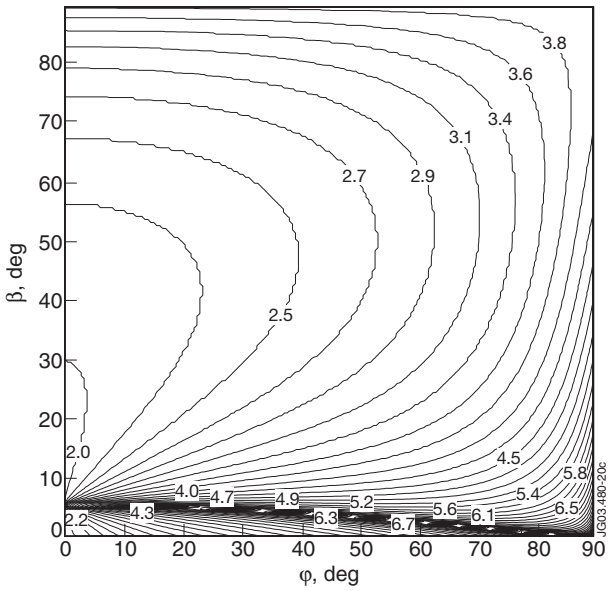

Figure 7: $\mathcal{L}n\ \{|\Phi(\eta_Z, \beta, \varphi)|\}$ at $\eta_Z = -0.1$, $\mathcal{L}_Z\,\eta_Z/\mathcal{L}_T > 0$.

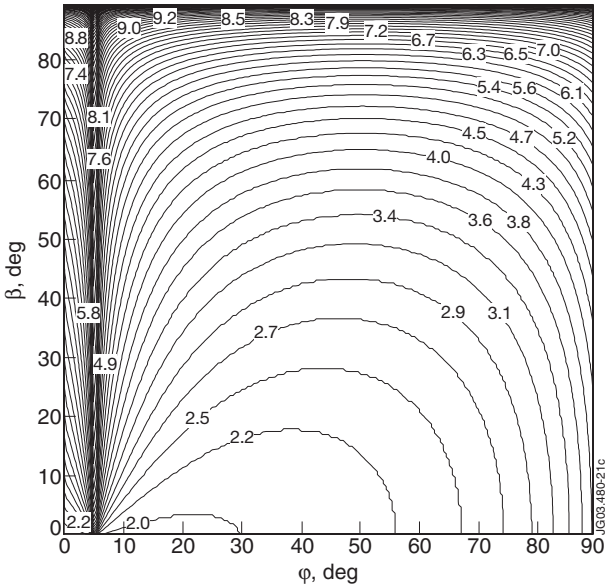

Figure 8: $\mathcal{L}n\ \{|\Phi(\eta_R, \beta, \varphi)|\}$ at $\eta_R = 0.1$, $\mathcal{L}_R\,\eta_R/\mathcal{L}_T > 0$.

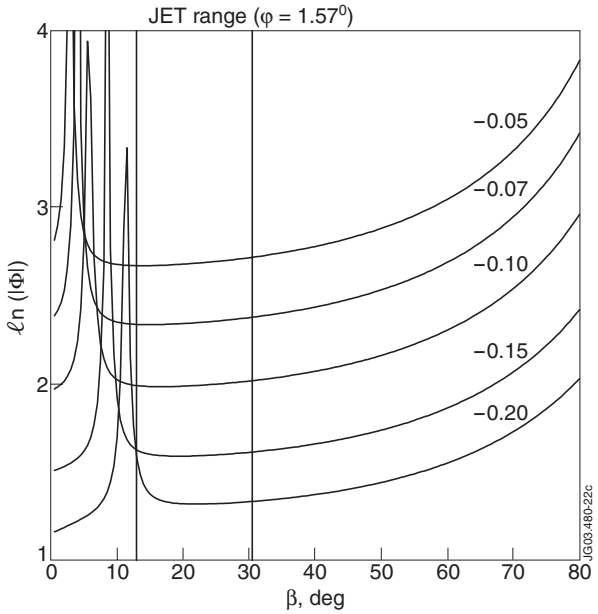

Figure 9: $\ell n\ \{|\Phi(\eta_Z, \beta)|\}$ for the geometry of the Li-beam system on JET. The values of η_Z are shown near the curves

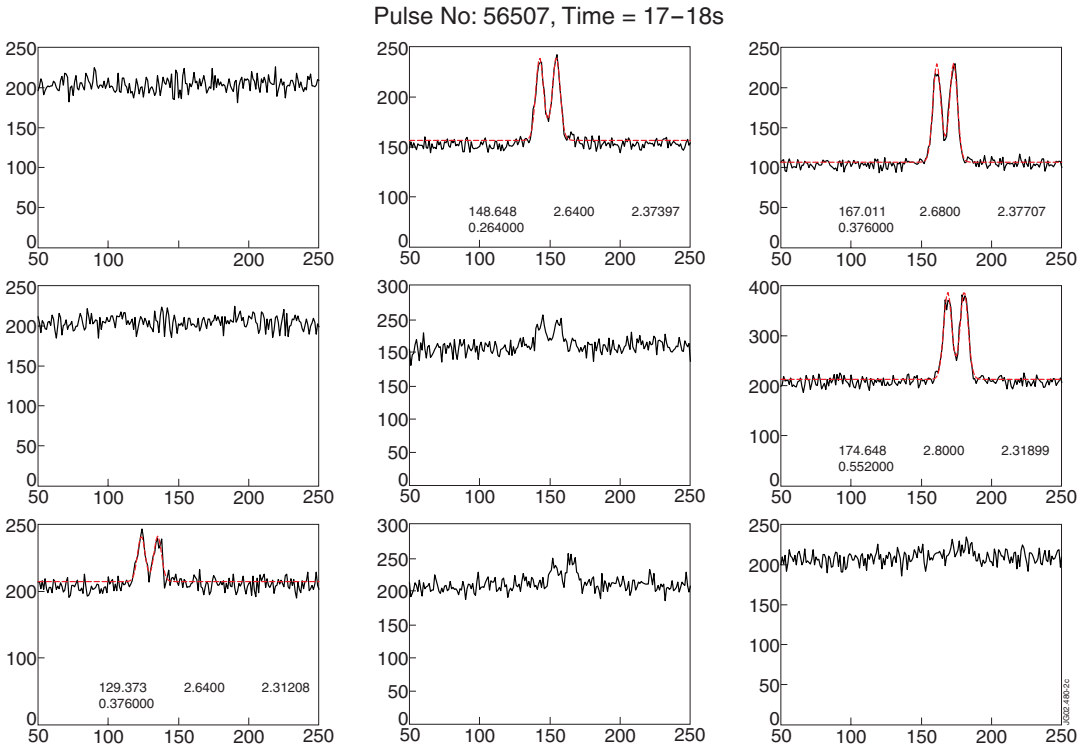

Figure 10: Li(2 ^{2}S-2 ^{2}P, λ_0=6707.85 Å)- emission from atoms with energy 29.5keV Spectra presented as functions of CCD pixel numbers for all nine spatial channels of the high resolution spectrometer SPEX1.25. Dispersion of the spectrometer is 0.082 Å/pix. Smooth lines are for fitting function. Parameters A_1, A_2 in pixels and A_4, A_5 in Tesla are indicated for the channels looking at the Li-beam.

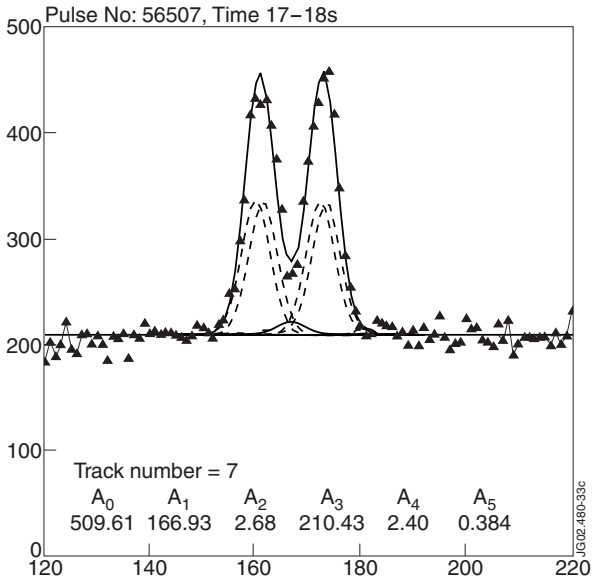

Figure 11: Maximum likelihood function and the parameters derived from the Least squares method. Contribution of 4σ- components and 2π - components are shown.

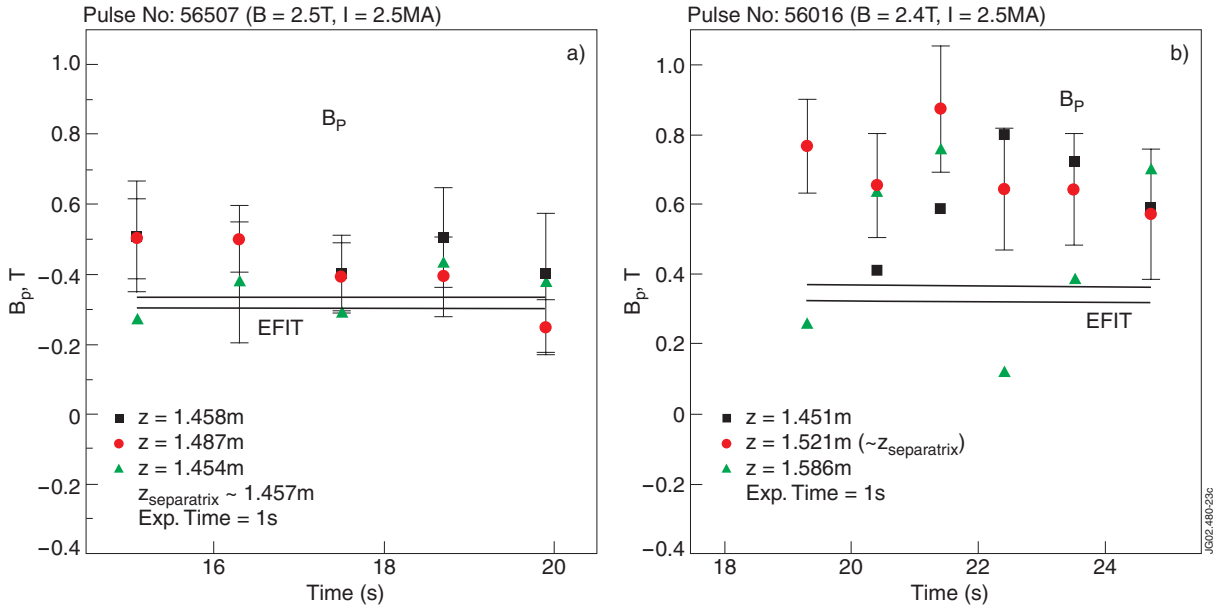

Figure 12: Time behaviour of the poloidal magnetic field in the vicinity of the separatrix. a) ohmic pulse, b) H-mode pulse, ELM frequency is 5Hz. z is the distance from the geometric midplane along the vertical beam line. EFIT equilibrium reconstruction is for the limiting points of the Z intervals presented and is based on measurements with coils and loops only. Error bars are from the deconvolution procedure described in section 3.2.

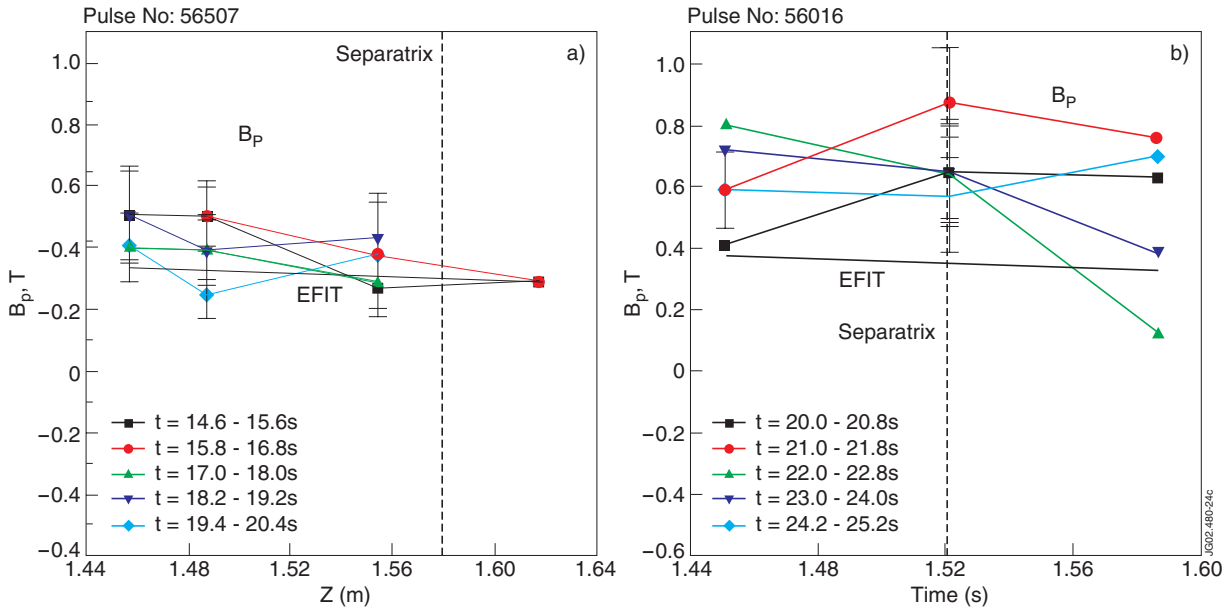

Figure 13: Spatial distributions of the poloidal magnetic field along the vertical beam line for the shots of figure 12.

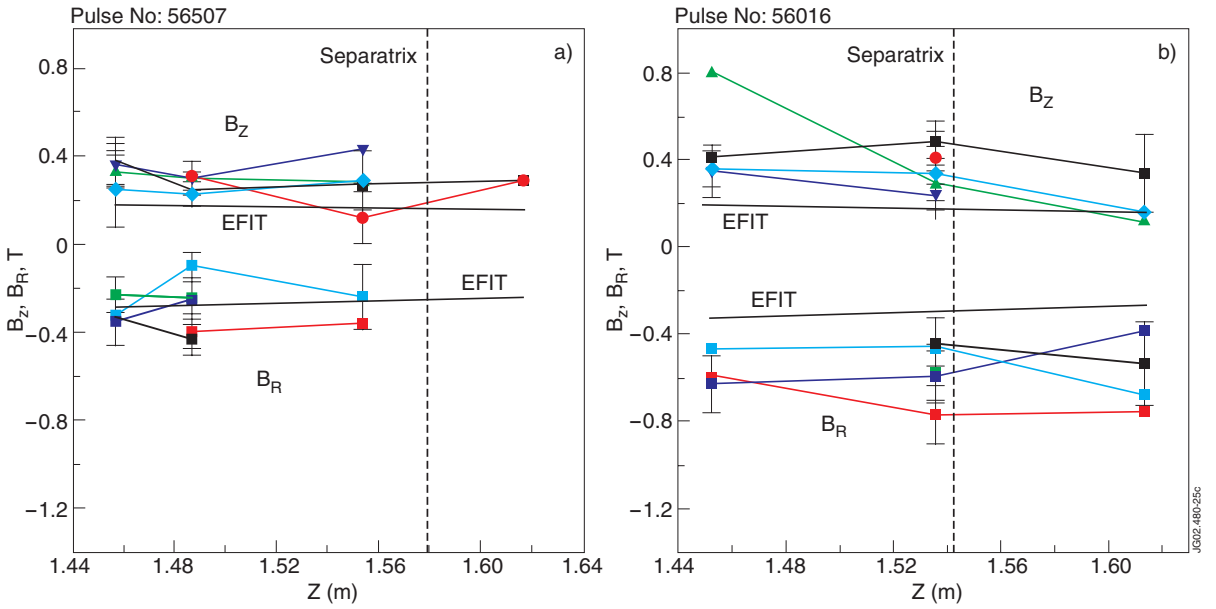

Figure 14: The same as in figure 13 but for the poloidal magnetic field components.

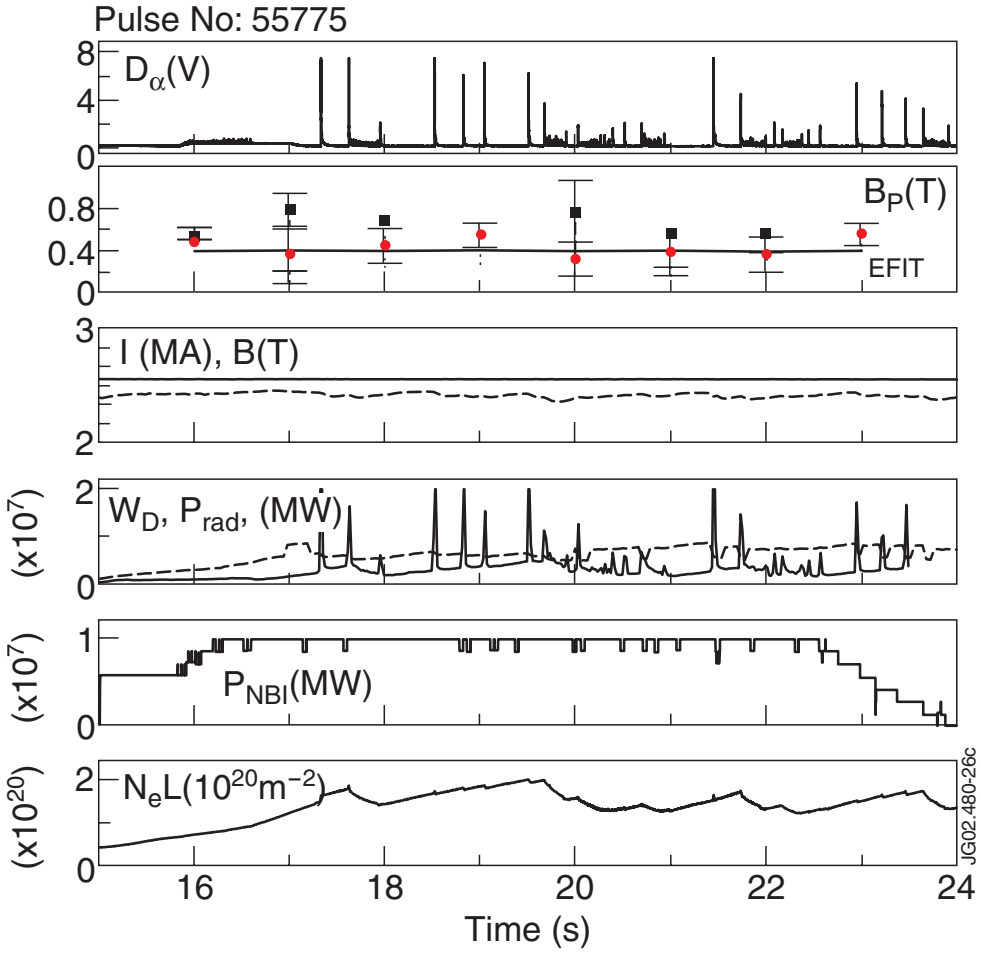

Figure 15: Time traces for a pulse with very infrequent ELMs. Boxes from top to bottom: D_α emission, B_P measured at points with distance of 6 (circles) and 10cm (squares) from the separatrix, total current and vacuum toroidal magnetic field at R=2.96m, diamagnetic energy and total radiated power, Neutral Beam heating power, line averaged density.

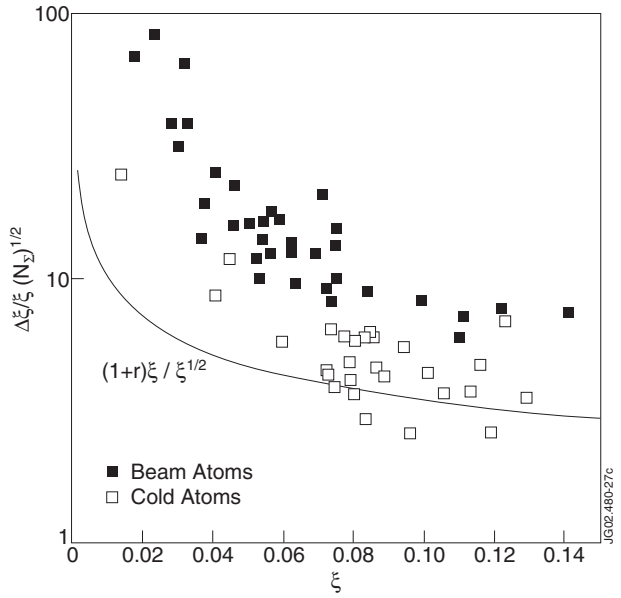

Figure 16. Uncertainty of ξ estimated from the measurement (squares). The statistical limit is shown by the solid curve.

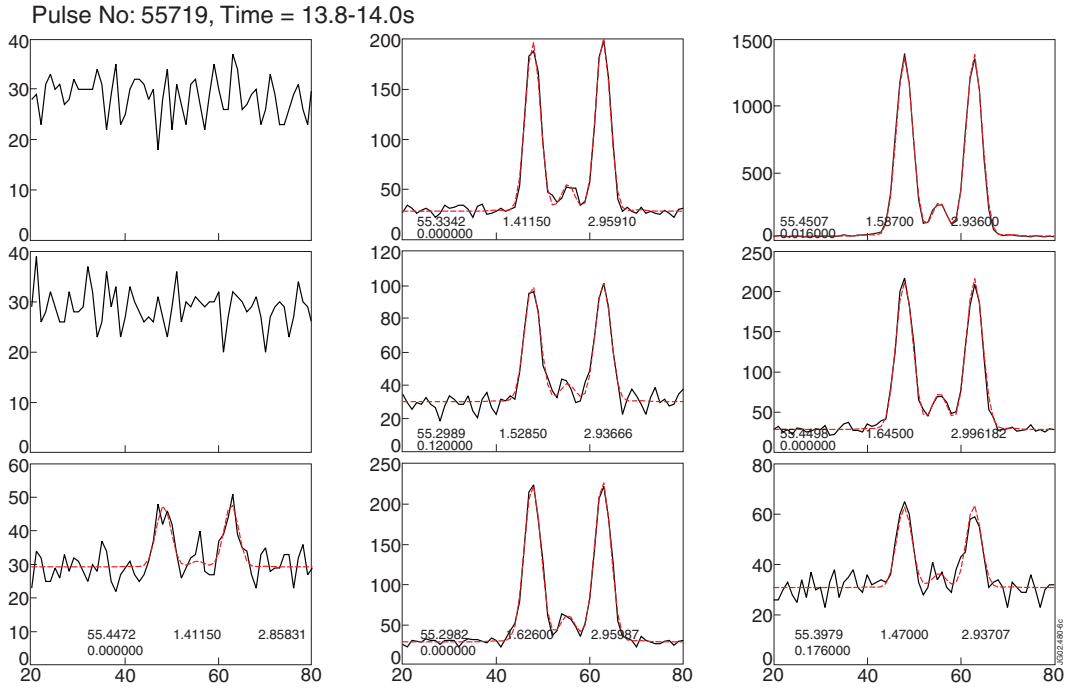

Figure 17: Li($2\,^2S$-$2\,^2P$, λ =6707.85 Å)- emission from cold atoms. Conditions of the measurement are similar to that in Figure 10. Smooth lines are for fitting function found under the assumption of a free fall trajectory for the flake. Parameters A_1, A_2 in pixels and A_4, A_5 in Tesla are indicated.

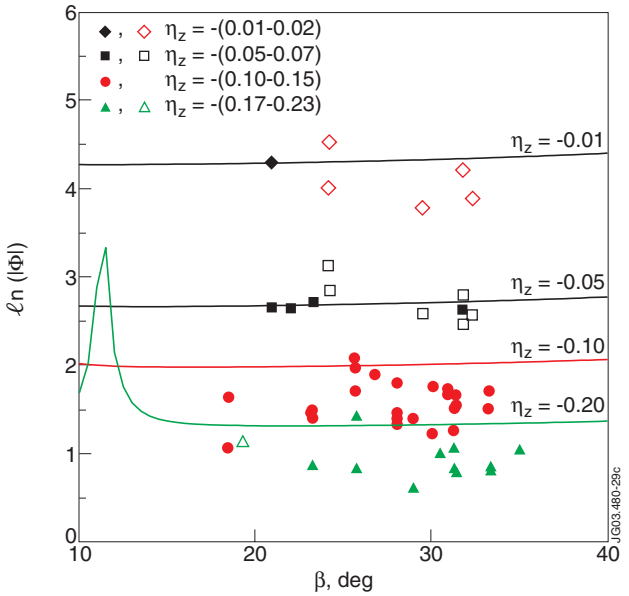

Figure 18: $\ell n(|\Phi|)$ calculated at $\varphi = 1.57^o$ (curves). Points are for the estimation from the measurement: $\ell n(|(\Delta B_Z/B_Z)\,(1+\xi)\sqrt{\xi}\,/\,(f(k)\Delta\xi)|)$. Open symbols are for the cold atoms.

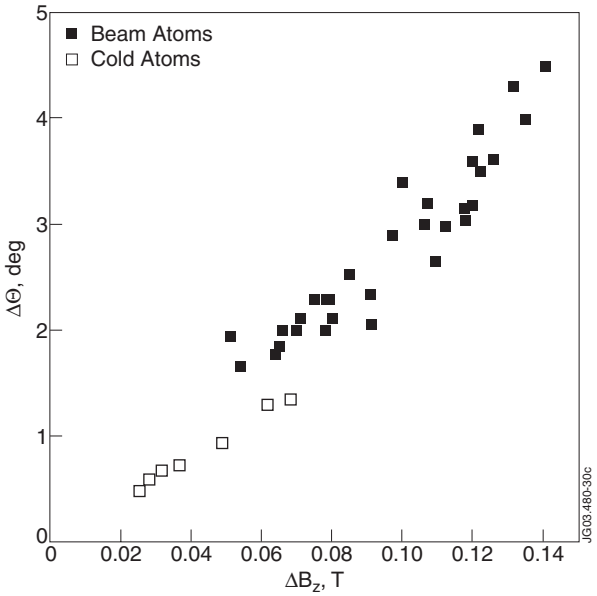

Figure 19: Accuracy for the B_Z and θ achieved in the measurements.

APPENDIX 1

GEOMETRY EXCLUDING UNCERTAINTY FOR INFERRED B

Three components of $\vec{B}$ are deduced from the measurement of ξ at two different inclination angles and measurement of $|\vec{B}|$. One uses the system of equations:

$$\begin{cases} B\,F_1 = B_T \ell_{T1} + B_R \ell_{R1} + B_Z \ell_{Z1} \\ B\,F_2 = B_T \ell_{T2} + B_R \ell_{R2} + B_Z \ell_{Z2} \\ B^2 = B_T^2 + B_R^2 + B_Z^2 \end{cases} \tag{1.1}$$

where $F_{1,2} = \cos\theta_{1,2}$.

The first two equations determine two conical surfaces for $\vec{B}$ around $\vec{\ell}_1$ and $\vec{\ell}_2$. The intersections of the surfaces give in the general case two possible directions for $\vec{B}$. The third equation does not differentiate between them. Nevertheless no uncertainty arises if the geometry of observation is chosen properly.

Without loss of generality we assume that $\left(\vec{\ell}_1 \times \vec{\ell}_2\right)_Z \neq 0$. Then the solution of (1.1) is

$$\begin{aligned} B_T &= \frac{1}{\ell_{T1}} (B\,F_1 - B_R \ell_{R1} - B_Z \ell_{Z1}), \\ B_R &= -\,a_R B_Z + B\,\frac{(F_2 \ell_{T1} - F_1 \ell_{T2}),}{\left(\vec{\ell}_1 \times \vec{\ell}_2\right)_Z} \\ B_{Z_{1,2}} &= -\,Q \pm \sqrt{Q^2 - P}\,, \end{aligned} \tag{1.2}$$

where

$$Q = B_T \frac{\ell_{T1} a_T}{A} + O(\eta), \quad P = 2BB_T \frac{\ell_{T1}}{A} (\eta_R \ell_{R1} + \eta_Z \ell_{Z1}) + O(\eta^2),$$

$$A = (\ell_{Z1} - a_R \ell_{R1})^2 + (1+a_R)\,\ell_{T1}^2\,, \; a_T = \frac{\left(\vec{\ell}_1 \times \vec{\ell}_2\right)_T}{\left(\vec{\ell}_1 \times \vec{\ell}_2\right)_Z}\,, \; a_R = \frac{\left(\vec{\ell}_2 \times \vec{\ell}_1\right)_R}{\left(\vec{\ell}_1 \times \vec{\ell}_2\right)_Z}$$

In tokamak plasmas we always have $|\eta_s| = |B_s/B_T| << 1$, where s stands for R or Z.

Therefore

$$\frac{P}{Q^2} \sim 2\eta << 1 \text{ and } B_{Z_{1,2}} \approx -\,Q \pm Q\left(1 - \frac{P}{2Q^2}\right),$$

if

$$|\ell_{T1}|, \left|\left(\vec{\ell}_1 \times \vec{\ell}_2\right)_T\right| >> |\eta_s|. \tag{1.3}$$

The solution $B_Z \approx -2Q \sim B_T$ must be omitted. The only valid solution for $B_Z = \eta_Z B_T$ is

$$B_Z = -Q + \sqrt{Q^2 - P} \approx -\,\frac{P}{2Q^2}\,,$$

The conditions (1.3) mean that angles between $\vec{B}_T$ and lines of sight $\vec{\ell}_1$ and $\vec{\ell}_2$ should not be too small ($>>|\eta_s|$) and at least for one line of sight this angle should not be too close to $\pi/2$. Fig.1.1 explains the results.

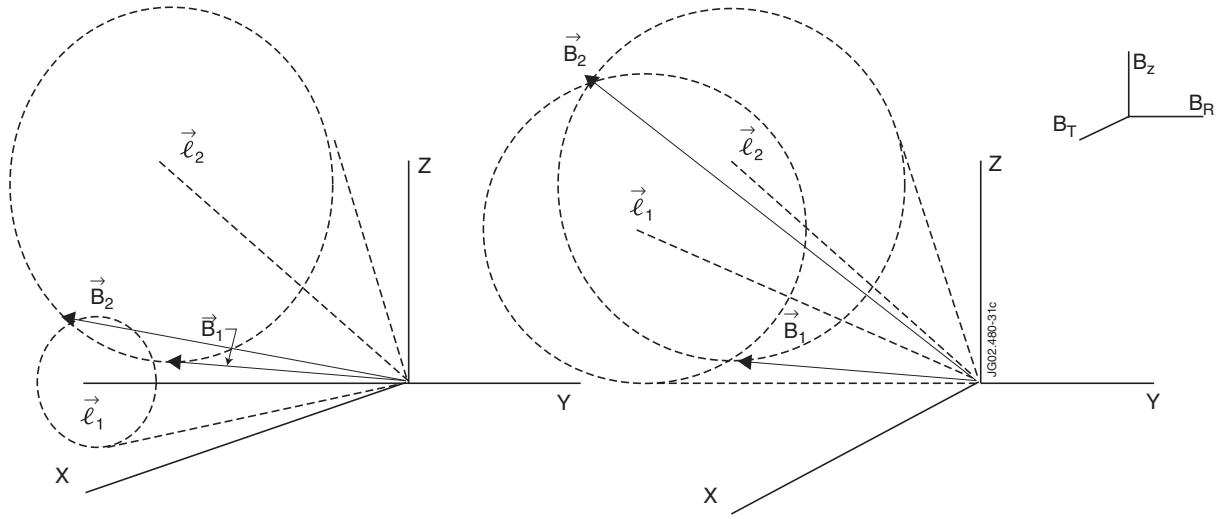

Figure 1.1. In the lefthand diagram, the angle between $\vec{\ell}_1$ and $\vec{B}$ is of order η. Both solutions $\vec{B}_1$ and $\vec{B}_2$ are possible. In the right hand diagram $\vec{B}_2$ must be omitted since it corresponds to $\eta_Z \sim 1$. The toroidal direction is along the X-axis.

APPENDIX 2

RELATIONSHIP BETWEEN MEASURED RATIO $\xi = J_\pi/J_\sigma$ AND INCLINATION ANGLE

Mirrors complicate the relationship between ξ and θ due to different reflectivity for P- ($k_{||}$) and S- ($k_\perp$) polarisation components (where the P-plane contains the incident ray and mirror normal and the S-plane is perpendicular to the P-plane). Since the measured intensities of the P- and S- components are:

$$J_P = k_{||} [J_\pi \sin^2\theta + J_\sigma \cos^2\theta) \cos^2 \gamma + J_\sigma \sin^2 \gamma] \quad (2.1)$$

$$J_S = k_\perp [J_\pi \sin^2\theta + J_\sigma \cos^2\theta) \sin^2 \gamma + J_\sigma \cos^2 \gamma] \quad (2.2)$$

one has

$$\xi(\theta) = \frac{C \sin^2 \theta}{1 + \cos^2 \theta + (1-k)\, \Psi(\beta, \varphi, k, \vec{B})} \quad (2.3)$$

where

$$\Psi(\beta, \varphi, k, \vec{B}) = \frac{\cos^2 \gamma - \sin^2 \gamma}{k \cos^2 \gamma + \sin^2 \gamma} \quad (2.4)$$

γ is the angle between ($\vec{\ell}$, $\vec{B}$)- plane and P-plane:

$$\cos \gamma = \left(\vec{e}_1 \bullet \vec{n}\right) = -\frac{B_Z \cos\beta + \sin\beta\, (B_R \sin\varphi + B_T \cos\varphi)}{B \sin\theta}$$

$$\sin \gamma = \left(\vec{e}_2 \bullet \vec{n}\right) = \frac{B_R \cos\varphi - B_T \sin\varphi}{B \sin\theta}$$

$\vec{e}_2$, $\vec{e}_1$ are the polarisation vectors in the ($\vec{\ell}$, $\vec{B}$)- plane and in the perpendicular plane, $\vec{n}$ is the P-plane normal, $\vec{\ell}$ is the sight line vector, $k = k_{//}/k_\perp$ J_π and J_σ are the intensities at $\theta = \pi/2$, $C = J_\pi/J_\sigma = (1+\Pi) / (1-\Pi)$, Π is the polarisation.

At small φ Eq.(2.3) reduces to Eq.(3). The most simple relationship exists at k=1:

$$\xi(\theta) = \frac{C \sin^2 \theta}{1 + \cos^2 \theta} \quad (2.5)$$

Since $\eta_z, \eta_R << 1$, $\Psi(\beta, \varphi, k, \vec{B})$ is a weak function of $\vec{B}$ if $\beta >> \eta_Z, \eta_R$ or $\varphi >> \eta_Z, \eta_R$. In zero-order approximation one has:

$$\cos^2 \gamma \approx \frac{\cos^2\varphi \sin^2\beta}{1 - \cos^2\varphi \cos^2\beta}, \quad \Psi \approx \frac{\cos^2\varphi \sin^2\beta - \sin^2\varphi}{k \cos^2\varphi \sin^2\beta + \sin^2\varphi}$$

The next-order approximation gives at $\beta >> \varphi$ ($(\vec{\ell}, \vec{B})$ - plane is approaching the P-plane):

$$cos^2 \gamma \approx 1 - \frac{\eta_R^2}{(\eta_Z cos\,\beta + sin\,\varphi)^2} \approx 1 \quad \Psi \approx \frac{1}{k} \quad if\ \beta >> \eta_Z, \eta_R \qquad ,$$

or in the reverse case $\beta << \varphi$ ($(\vec{\ell}, \vec{B})$- plane is approaching the S-plane):

$$cos^2 \gamma \approx \eta_Z^2 (1 + (\cos \varphi + \eta_R \sin \varphi)^2) << 1, \quad \Psi \approx -1 \quad \text{if } \varphi >> \eta_Z, \eta_R$$

APPENDIX 3

MEASUREMENT OF THE PARAMETERS $\{\beta_i\}$, φ, C, k

The parameters in Eqs.(2)-(3) are measured in-situ using the Li($2s\ ^2S - 2p\ ^2P$)- emission of the beam from plasma or deuterium gas. The last is a powerful method for alignment of the periscope system. Of crucial importance is the use of a spectrometer that enables a measurement of the Doppler shifts $\{\Delta_D\lambda_i\}$ for all spatial channels.

The set of β- angles $\{\beta_i\}$ is derived straightforwardly from

$$\Delta_D\lambda_i = \lambda_0 \frac{v_{beam}}{c} \sin\beta_i \qquad (3.1)$$

The results of the deconvolution procedure (section 3.2) show that $\Delta_D\lambda_i$ is measured with accuracy of ~0.3 pixel or 0.025Å. It provides an accuracy of ~ 0.01^0 for the angles β_i.

The measurement of the other parameters requires a toroidal B_T and vertical B_Z magnetic field application. The best way to determine the angle φ is to find a minimum of the ratio ξ by varying B_Z or alternatively measuring ξ at different angles β at fixed B_Z. The ξ (Eq.2.3) has a minimum at[3.1]

$$\tan\beta = -\frac{2\eta\cos\varphi}{1-\eta^2} \qquad (3.2)$$

where $\eta = B_Z / B_T$ ($\eta < 0$ and $\beta, \varphi > 0$ are assumed). This method allows the measurement of φ without knowledge of C and k.

The parameter C[3.2] can be determined from the measurement of ξ at $\sin\beta = \tan\varphi$ in gas with B_T ($B_Z = 0$). At such condition the ξ does not depend on k ($\Psi(\beta, \varphi, k, \vec{B}) = 0$):

$$\xi_{\sin\beta=\tan\varphi} = \frac{C(1-\cos 2\beta)}{2}\ , \qquad (3.3)$$

Finally, knowing $\{\beta_i\}$ and C one can infer $k(\beta)$ for each spatial channel using Eq.(2.3)[3.3].

[3.1] We consider a scheme with the possibility of measurement along $\vec{B}_T$ since $\eta \ll 1$. If a perpendicular line of sight is possible ($\vec{\ell} \perp \vec{B}_T$) one should find a maximum of ξ that corresponds to $\tan\beta = \cos\varphi/\eta$.

[3.2] Parameter C is different in gas and plasma. Moreover C depends on the position of the source in the plasma (i.e. on angle β) due to influence of the electrons on the polarisation (see Chapter 2.3).

[3.3] Everywhere we assume that the beam is in the optical plane of the periscope.

APPENDIX 4

POPULATION OF THE Li(2pm) STATES DUE TO COLLISIONS WITH PROTONS

The population of the Li(2pm)- states P_m^i due to proton impact has been calculated using the close coupling approach and expansion of the initial and final states over atomic orbitals. The expansion includes 65 orbitals centred on the proton and 64 orbitals centred on the lithium atom, thus all inelastic reaction channels are represented. The absolute cross-sections for the excitation process were published earlier [6]. The relative population of the 2pm- states as a function of the impact energy is presented in Fig.4.1.

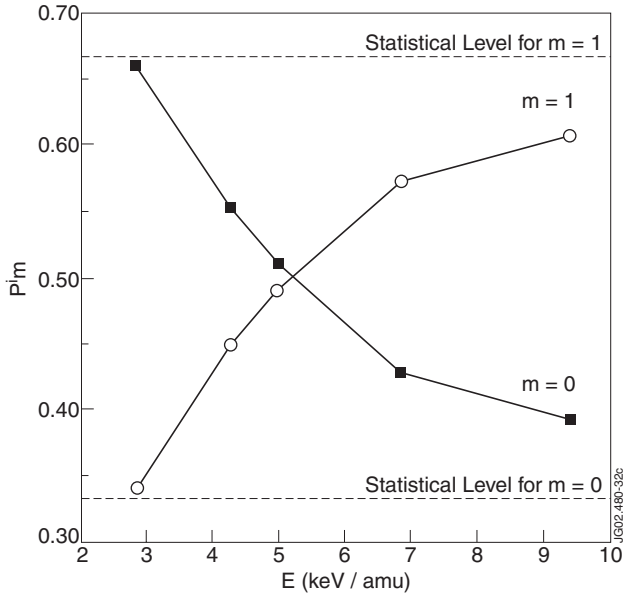

Figure 4.1: Population of Li(2pm)- states due to excitation of Li(2s) by proton impact. P(m=1) = P(m=-1) + P(m=+1). Quantisation axis is parallel to the trajectory of the projectile.

At low energies the m=0- state is predominantly populated, explaining the polarisation of the 2s ^{2}S – 2p ^{2}P- radiation. The effect becomes negligible when the collision velocity exceeds the orbital velocity of the electron in the lithium atom (E > 6.5 keV/amu).

The calculation is done in the so-called collision system (or beam frame) with the quantisation axis directed along the trajectory of the projectile. For the polarisation analysis the 2pm-states from the beam frame are to be projected into the frame with the quantisation axis directed along the magnetic field vector (if $\mathbf{v}_{beam}$ is not parallel to **B**). The latter has been performed using the formalism described in [7].